

Timing Analysis of the Isolated Neutron Star RX J0720.4–3125 Revisited ^{*}

Mark Cropper¹, Frank Haberl², Silvia Zane¹, Vyacheslav E. Zavlin²

¹*Mullard Space Science Lab, University College London, Holmbury St. Mary, Dorking, Surrey, RH5 6NT, UK*

²*Max Planck Institut für Extraterrestrische Physik, Giessenbachstrasse, D-85748 Garching, Germany*

Received:

ABSTRACT

We present a reanalysis of the X-ray data for RX J0720.4–3125 presented in Zane et al. (2002), using more data recently available from *XMM-Newton* and *Chandra*. This analysis also corrects the *ROSAT* data used in that paper to the TDB time system, incorporates the revised *XMM-Newton* barycentric correction available since then, and corrects the definition of the instantaneous period in the maximum likelihood periodogram search. However, we are now unable to find a single coherent period that is consistent with all *ROSAT*, *Chandra* and *XMM-Newton* datasets. From an analysis of the separate datasets, we have derived limits on the period change of $\dot{P} = (1.4 \pm 0.6) \times 10^{-13}$ s/s at 99% confidence level. This is stronger than the value presented in Zane et al. (2002), but sufficiently similar that their scientific conclusions remain unchanged. We examine the implications in more detail, and find that RX J0720.4–3125 can have been born as a magnetar provided that it has a young age of $\sim 10^4$ yr. A more conservative interpretation is that the field strength has remained relatively unchanged at just over 10^{13} G, over the $\sim 10^6$ yr lifetime of the star.

Key words: Stars: neutron; stars: oscillations; pulsars: general; magnetic fields.

1 INTRODUCTION

RXJ0720.4–3125 is a nearby, isolated neutron star (INS) originally discovered with *ROSAT* during a systematic survey of the Galactic plane by Haberl et al. (1997). A clear modulation of the X-ray intensity is detected at a period of 8.391 s, which identifies the spin velocity of the neutron star.

RX J0720.4–3125 is, so far, the isolated neutron star with best studied timing properties. Its proximity and relatively high brightness made possible not only to measure the spin period, but also to study the period changes over a long-term. This is crucial, since the positive detection of spin-up or spin-down phases can shed light on the mechanisms that regulate the neutron star interaction with its surroundings. A large positive spin-down can indicate magnetodipolar breaking, leading in turn to an estimate of magnetic field strength and star spin down age. In the attempt to measure a secular period change, Zane et al. (2002, hereafter Z02) recently undertook a comprehensive timing analysis of *ROSAT*, *BeppoSAX*, *Chandra* and *XMM-Newton* data spanning a total period of ~ 7 yrs. Independently, a similar

analysis based on an additional *Chandra* dataset, but without the *XMM-Newton* data, was presented by Kaplan et al. (2002, hereafter K02). Although the two studies agreed in their main conclusion that the period change was less than $\sim 3 \times 10^{-13}$ s/s, it was evident that there were inconsistencies in the details of the analysis which have implications for further studies. The arrival times computed by the two groups were different. K02 also raised theoretical concerns about the validity of the *coherent* analysis of the entire dataset carried out by Z02. That was the only method that, at that time, permitted the (positive) sign of the period change to be constrained. In fact, the phase-incoherent analysis presented by Kaplan et al. (2002) still leads to a large uncertainty in \dot{P} , and does not permit the discrimination between positive and negative spin-down.

The above-mentioned inconsistencies have motivated us to undertake a complete revision of the solution. At the time Z02 was published, timing inconsistencies between *XMM-Newton* and radio data on other pulsars had come to light (Kuster et al. 2001). This was traced to an error in the *XMM-Newton* Science Analysis System (SAS) task *barycen* before version 13.1 [the spacecraft position vector was constructed as (x, y, y) instead of (x, y, z)]. Although we argued in Z02 that any effect on the coherent analysis was small, we nevertheless performed a reanalysis of the *XMM-Newton* data to check, and also to investigate whether this corrected

^{*} Based on observations obtained with *XMM-Newton*, an ESA science mission with instruments and contributions directly funded by ESA Member States and the USA (NASA).

the inconsistencies with the K02 analysis. We found indeed that the effect was negligible. The implication is therefore that the inconsistencies between the Z02 and K02 analyses remained.

We have therefore undertaken a complete reanalysis of the dataset to investigate and eliminate these inconsistencies. This has brought to light that the times used for the *ROSAT* data in both the Z02 and K02 studies are in UTC rather than TDB as used for *Chandra* and *XMM-Newton*; the times of arrival (ToAs) in K02 are incorrectly calculated; and that the formula used to calculate the instantaneous phase was incorrect in Z02. Substantial new datasets are also available from both *XMM-Newton* and *Chandra* which permit a more comprehensive investigation into the period evolution. We report here the results of this reanalysis.

2 NEW OBSERVATIONS AND REVISIONS

We refer the reader to Z02 and K02 for the details of the previous observations, and comment here largely only on those aspects which have changed. The table of observations is given in Table 1.

2.1 *XMM-Newton* Data

RX J0720.4–3125 has been observed four times by *XMM-Newton*, in revolutions 78, 175, 533/534 and 622. This is a substantial increase over that available to Z02.

In Z02, for revolution 78 (X00a in Z02), special arrangements (*tcs_fix*) were made to ensure the timing accuracy of the data in the absence of a full observation data file (ODF). In the intervening period, the observation has been reprocessed in the *XMM-Newton* pipeline, so that the standard observation data file (ODF) is now available. We used SAS 5.2 *odfingest* to prepare the ODFs and were also assisted by U. Lammers at ESA who ran a more recent (not then public) version. Nothing unexpected with regard to timing could be found in the logs or in a direct inspection of the ODF time correlation and orbit data. In running the pipelines (SAS *emchain* and *epchain*), we tracked down timing correction extrapolation warnings in EPIC-pn to anomalous auxiliary data within the first 100 frames after the exposure start in some quadrants, causing the computation of the time tags to fail. This problem was fixed by U. Lammers using software which was later released in SAS 5.3.2. Also in EPIC-pn for the X00b data, we corrected the 1 s errors in the frametime as described in Z02. For the EPIC-mos data we found some timing warnings referring to non-increasing times: these were flagged automatically and not included in the later selection procedure we used to create the extracted event lists. In other regards, the extraction was performed as in Z02.

The rev. 533/534 observations of RX J0720.4–3125 were made for calibration purposes on 2002 Nov 6–9. Extending over 3 days, these data can provide tighter constraints on the period determinations than the earlier observations. The EPIC-pn data only were extracted using the procedures described in Z02, with the same extraction parameters. SAS v5.3.2 was used to process the events. Corrections were applied for the 1 s frametime errors as described in Z02. Rev

622 observations were also made for calibration purposes on 2003 May 2. These were processed as for rev 533/534.

For both old and new datasets the barycentric correction was carried out using SAS *barycen* version 13.1 and 13.2.

2.2 *ROSAT* Data

Despite that the *ROSAT* data had been processed in two different ways in Z02 (as a double check, using both the *ROSAT* EXSAS software system and FTOOLS), an error was made in not converting the time system from UTC to TDB in order to relate these observations to the *XMM-Newton* and *Chandra* data, both of which use the TT/TDB system. The timings for the *ROSAT* data were therefore recomputed, using the *convert/utc_tdb* task in EXSAS. The absolute timing of the 1998 *ROSAT* data is uncertain, which prevents their use in any coherent analysis (Z02).

We have also extracted the data for RX J0720.4–3125 from the *ROSAT* All Sky Survey. These data suffer from relatively low count rates because of vignetting away from the field centre, and also the obscuration from the PSPC detector support grids. On the other hand the duration of the observations is several days (2.07 d) days, so they potentially provide a good constraint on the period determination. Finally we have also extracted early HRI observations taken in 1994 May. The source is near the edge of the detector area, and the observation yields only a small number of counts. Nevertheless, as for the RASS data, the duration of the observation provides some useful constraints.

2.3 *BeppoSAX* Data

In Z02, the *BeppoSAX* observations were not directly used in the period analysis, but were folded on the derived periods from the remaining data to check the consistency of the period solution. As the FTOOLS *Earth2Sun* correction used in Z02 did not apply the *BeppoSAX* clock correction, the *BeppoSAX* data have been reprocessed using the SAX Data Analysis System and the correction recomputed using the *baryconv* task in SAX DAS (kindly performed by M. Feroci). It was confirmed by T. Oosterbroek (private communication) that the SAX timings after this operation are in the TDB system.

2.4 *Chandra* Data

Since the work of Z02, *Chandra* observations made in 2001 December 4–6 have become publically available. These observations were reported in K02. In this work, we used the *Chandra* data on RX J0720.4–3125 collected in four observations of 2001 December 4–6, with effective exposures of 15.0, 10.6, 4.1 and 1.9 ks. The observations were conducted with the Advanced CCD Imaging Spectrometer (ACIS-S) operated in Continuous Clocking mode. This observational mode provides a 2.9 ms time resolution by means of sacrificing spatial resolution in one dimension. In total, we used 66,822 counts extracted from segments of a 3''.44 width in the one-dimensional images of the source, in the 0.1–1.0 keV range. The times of arrival were corrected for the dither and the Science Instrument Module motion as described in detail

Date	Observatory	Instrument	Exposure identification	Exposure duration (s)	Effective exposure (s)	Label
1990 Oct 11	<i>ROSAT</i>	PSPC		178840		RASS
1993 Sep 27	<i>ROSAT</i>	PSPC	rp300338n00	11980	3221	R93
1994 May 11	<i>ROSAT</i>	HRI	rh201733n00	173237	7402	R94
1996 Apr 25	<i>ROSAT</i>	HRI	rh300508n00	7743	3125	R96a
1996 May 7	<i>ROSAT</i>	HRI	rh180100n00	7838	3566	R96b
1996 Sep 27	<i>ROSAT</i>	HRI	rh300508a01	1498	1409	R96c
1996 Nov 3	<i>ROSAT</i>	HRI	rh400884n00	65698	33569	R96d
1997 Mar 16	<i>BeppoSAX</i>	LECS	LECS_20079001	99418	17235	S97
1998 Apr 20	<i>ROSAT</i>	HRI	rh400944n00	460195	3566	R98
2000 Feb 1	<i>Chandra</i>	HRC-S(LETG 1st order)	348+349+745	305528	37635	Ch00
2000 May 13	<i>XMM-Newton</i>	MOS1 + thin filter	0124100101-001	61352	61648	X00a
		MOS2 + thin filter	0124100101-002	61648	61648	
		PN + thin filter	0124100101-003	52305	52305	
2000 Nov 21	<i>XMM-Newton</i>	MOS1 + medium filter	0132520301-007	17997	17997	X00b
		MOS2 + medium filter	0132520301-008	17994	17994	
		PN + medium filter	0132520301-003	25651	25651	
2001 Dec 4	<i>Chandra</i>	ACIS-S	2771–2774	171243	31532	Ch01
2002 Nov 6	<i>XMM-Newton</i>	PN + thin filter	0156960201-003, 0156960401-003	208582	58554	X02
2003 May 2	<i>XMM-Newton</i>	PN + thick filter	0158360201-023	72793	72793	X03

Table 1. The *ROSAT*, *BeppoSAX*, *Chandra* and *XMM-Newton* observations of RXJ0720.4–3125 used in this paper.

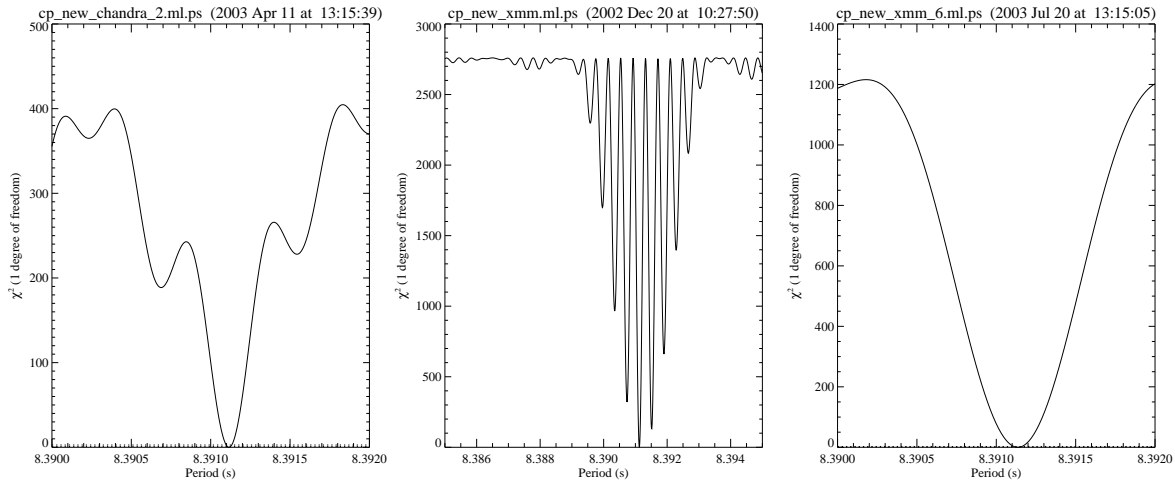


Figure 1. The MLPs for the Ch01 data (left), the X02 data (center) and the X03 data (right). The 68 percent 1σ confidence levels are set from $\Delta\chi^2 = 1$, and are not discernible on these plots.

in Zavlin et al. (2000), and transformed to the Solar System Barycenter using the *axBary* tool of the CIAO package¹.

3 MODEL REVISIONS

Z02 (equation A5) defined the instantaneous period to be

$$P(t) = P_0 + \dot{P}(t - t_0), \quad (1)$$

where P_0 is the period at $t = t_0$ and \dot{P} is the period change. This period was substituted in the model prediction used in the Maximum Likelihood Periodogramme (MLP) (equation A4 in Z02)

$$I(t) = a_0[1 + A \cos(2\pi t/P(t) + \theta_0)], \quad (2)$$

where A is the normalised amplitude and θ_0 is the phase.

This substitution is a rough approximation: as the cosine argument in equation (2) is a phase corresponding to the orientation of the neutron star, the cumulative outcome of the past history of the period variations is not negligible.

¹ <http://asc.harvard.edu/ciao/>

The definition of angular frequency is:

$$\omega(t) = \frac{2\pi}{P(t)} = \frac{d\phi}{dt},$$

thus, substituting $P(t)$ from equation (1), the phase at time t is

$$\phi(t) - \phi(t_0) = 2\pi \int_{t_0}^t \frac{1}{P_0 - \dot{P}t_0 + \dot{P}t} dt. \quad (3)$$

In our prescription, \dot{P} is constant, so this can be integrated analytically to

$$\phi(t) - \phi(t_0) = \frac{2\pi}{\dot{P}} \ln \frac{P(t)}{P_0}. \quad (4)$$

Accordingly, the model prescription should be revised from equation (2) to

$$I(t) = a_0 \left[1 + A \cos\left(\frac{2\pi}{\dot{P}} \ln \frac{P(t)}{P_0} + \theta_0\right) \right], \quad (5)$$

where $P(t)$ is as defined in equation (1) and all of the timing and phase zero points are included in θ_0 .

The calculation of the phase in the MLP via equation (5) is slower than that previously done via equation (2), and care is required in order to minimise the numerical errors resulting from the calculation of the logarithm of a number close to unity. In particular in the case where $\dot{P} = 0$, the solution of equation (3) is $\phi(t) - \phi(t_0) = 2\pi(t - t_0)/P_0$ and then the intensity model is simply

$$I(t) = a_0 [1 + A \cos(\frac{2\pi t}{P_0} + \theta_0)]. \quad (6)$$

It could be argued that in the presence of constant torques, a constant $\dot{\nu}$ assumption is more valid than a constant \dot{P} . In this case the accumulated phase is $\phi(t) - \phi(t_0) = 2\pi\nu(t) + 2\pi\dot{\nu}t^2/2$. In practise we checked that, for $\dot{P} = 5 \times 10^{-13}$ s/s (Z02, K02), the accumulated phase difference over ten years between these assumptions is < 0.5 percent and therefore negligible. The two assumptions give consistently similar results, and this also implies that a small second derivative term $\ddot{\nu}$ (of the kind $\ddot{\nu} = 2\dot{P}/P^3 - \ddot{P}/P^2$) does not affect the solution. With the increase in the time baseline, however, it will become increasingly possible to distinguish between the models. In order to facilitate comparison with Z02 and K02 we retain the constant \dot{P} model here.

4 PERIOD DERIVATIVE FROM THE INDIVIDUAL DATASETS

The new data allow a more accurate determination of the period derivative using a conventional least squares fit to the individual periods than was possible in Z02. This is because the quality of the recent data permit a breaking of the ambiguities that were present in the dataset used in Z02 caused by the alias patterns in the *ROSAT* data. We perform a new analysis, both in order to provide a robust estimate of \dot{P} which in itself is now sufficiently accurate to provide scientific constraints, and in order to provide a defined region of parameter space for the more computationally intensive phase-coherent analysis which follows.

Given the ad-hoc nature of the epochs at which observations have been taken, it is necessary to proceed in a

step-wise fashion. First the best fitting periods and their uncertainties have been derived for the new *Chandra* (Ch01) and *XMM-Newton* (X02, X03) datasets (Figure 1), and also the S97 and the RASS datasets using a MLP as in Z02. These were added to those derived in Z02. The full list is given in Table 2. The first stage is to use the *XMM-Newton*, Ch01, R93 and R96d datasets to determine unequivocally the appropriate alias peaks in the Ch00 data and the R98 data, since in these individual datasets there is no question of the period determination. We performed a weighted least squares fit using these data, with parameters P_0 and \dot{P} and the extrema of the 99 percent confidence ellipsoids determined. The result is shown in Figure 2 (top). The solid line is the best fit $P = P_0 + \dot{P}t$, while the dotted lines bound the range in P permitted from the 99 percent extrema. Also shown are the aliases of the period determinations for the R96 and Ch00 data. It is clear that only the aliases corresponding to $P \sim 8.3911$ s are consistent with the least squares fit. These indeed correspond to those selected in Z02 and K02, but this (at least in Z02) relied on the correspondence of these peaks in the R98 and Ch00 MLPs.

It is now possible to include the periods for these peaks in the least squares fit and repeat the process. The result is shown in Figure 2 (middle). Also shown are the aliases of the combined R96a and R96b determinations: these are short runs but have a convenient two-week separation. Again from the 99 percent confidence range, the central alias at $P \sim 8.3911$ s is the only acceptable period. The 99 percent confidence interval changes slightly if we include the RASS period determination, but the selection of the aliases is unaffected. This in turn can be used to further constrain the fit, and to determine which alias should be selected from the combined R96c and R96d data, which have a 1 month separation. This is shown in Figure 2 (bottom), where the 99 percent confidence limits identify the alias at 8.391095 s as the appropriate period. Again, the RASS data can be included without any change to the alias selection. Including the period determined from this alias, the least confidence intervals in the P_0, \dot{P} plane are shown in Figure 3.

The outcome of this analysis is that the 99 percent confidence interval for the \dot{P} term lies in the range 0.70×10^{-13} to 2.10×10^{-13} s s⁻¹, with the 68 percent interval being 1.05×10^{-13} to 1.75×10^{-13} s s⁻¹. This is consistent with (but more accurate than) the incoherent analyses by Z02 and K02, and establishes that RX J0720.4–3125 is *spinning down*.

5 PERIOD DERIVATIVE FROM A COHERENT ANALYSIS

The change to the model used in the MLP noted above, together with the revised *ROSAT* timings (unimportant in the incoherent analysis above) means that the coherent period analysis in section 4.3 of Z02 must be revised – and indeed the 99 percent confidence limits in Figure 3 exclude all of the four identified P_0, \dot{P} pairs in their table 3.

5.1 Individual Satellites

As explained in Z02, the time taken to compute coherent 2-dimensional MLPs for a dataset of this size is prohibitive,

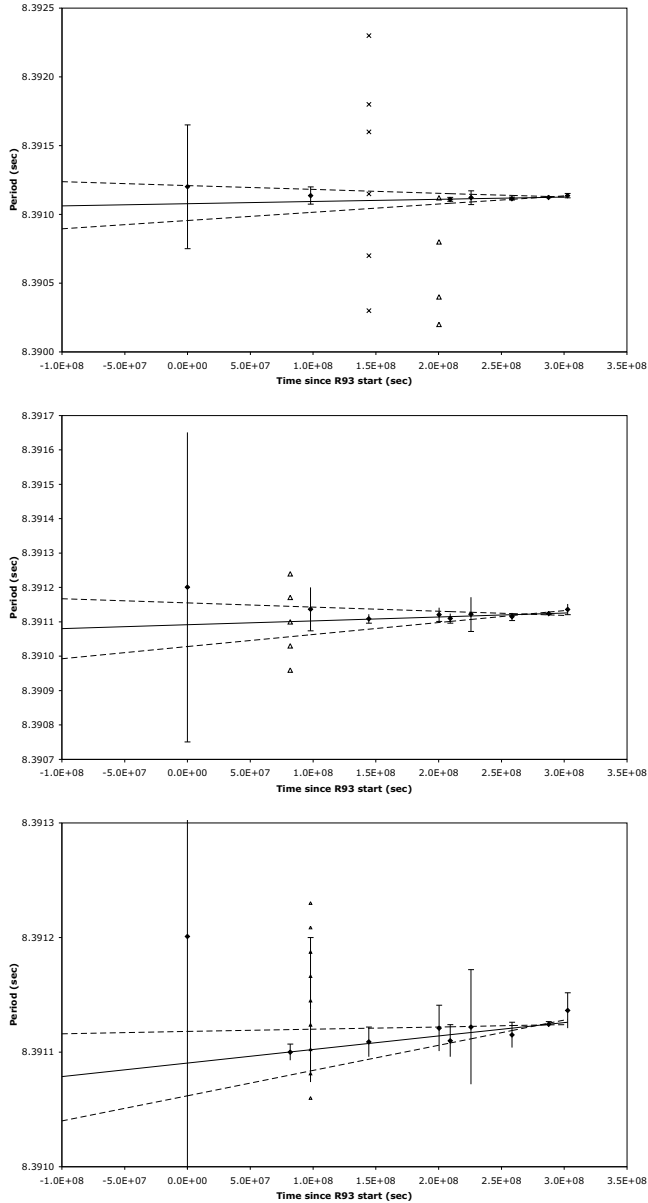


Figure 2. The periods as derived from the MLPs of the *XMM-Newton*, Ch01, R96d and R93 datasets (Table 2) shown as a function of time since the start of the R93 data. Error bars show 1σ uncertainties. The solid line is the best linear fit with dotted lines showing the 99% confidence interval. The period aliases for the R98 and Ch00 data are also shown. Only a single alias peak is admissible in each case (top). The best linear fit including the selected R98 and Ch00 aliases. Also shown are the period aliases from the combined R96a and R96b data. Only a single alias peak is admissible (centre). The best fit including the selected aliases from the R96a and R96b data. Also shown are the period aliases from the combined R96c and R96d data. Again, only a single alias peak is admissible within the 99% confidence range (bottom).

so that it has to be performed in stages. This can be done in several ways. Here we have analysed the *ROSAT*, *Chandra* and *XMM-Newton* datasets separately to start with. This avoids any residual difficulties in relating the different time systems used for the different satellites, or from any different assumptions in the data reduction software.

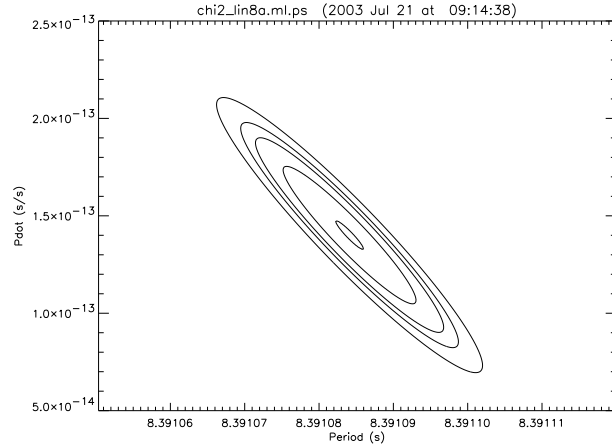


Figure 3. The 99%, 95%, 90% and 68% confidence interval contours in the $[P_0, \dot{P}]$ plane for the data in Figure 2 (bottom), and including the selected aliases from the R96c and R96d combined data. The central contour is drawn only to identify the minimum in the χ^2 plane.

Dataset	Period (s)	ToA (MJD)
RASS	8.390935 ± 0.000055	$48176.0202551 \pm 0.0000059$
R93	8.39120 ± 0.00045	$49257.2547035 \pm 0.0000028$
R94	8.39065 ± 0.00005	$49484.0535939 \pm 0.0000092$
R96a	8.3913 ± 0.0008	$50198.6873653 \pm 0.0000031$
R96b	8.3925 ± 0.0015	$50210.5563095 \pm 0.0000058$
R96a+b	8.391100 ± 0.000007	$50204.6220263 \pm 0.0000039$
R96c	8.392 ± 0.025	$50353.9975527 \pm 0.0000064$
R96d	8.391137 ± 0.000063	$50391.3007509 \pm 0.0000016$
R96c+d	8.391095 ± 0.000005	$50372.8348286 \pm 0.0000017$
S97	8.39113 ± 0.00012	$50523.7056342 \pm 0.0000040$
R98	8.391109 ± 0.000013	$50925.6882151 \pm 0.0000036$
Ch00	8.391121 ± 0.000020	$51577.0395669 \pm 0.0000026$
X00a PN	8.391110 ± 0.000014	$51677.4067206 \pm 0.0000003$
X00a MOS1	8.391110 ± 0.000047	$51677.4688770 \pm 0.0000010$
X00a MOS2	8.391113 ± 0.000034	$51677.4712089 \pm 0.0000007$
X00b PN	8.391122 ± 0.000050	$51869.9571032 \pm 0.0000006$
X00b MOS1	8.391060 ± 0.000170	$51869.9949797 \pm 0.0000012$
X00b MOS2	8.390850 ± 0.000190	$51869.9949796 \pm 0.0000014$
Ch01	8.391115 ± 0.000011	$52248.6768196 \pm 0.0000008$
X02 PN	8.391124 ± 0.000002	$52585.9688278 \pm 0.0000003$
X03 PN	8.391136 ± 0.000015	$52761.9950590 \pm 0.0000004$

Table 2. The periods and ToAs derived from the individual datasets.

In each case we have searched the $[P_0, \dot{P}]$ plane in the region within the 99% confidence intervals in Figure 3, using the 2-dimensional MLP as described in Z02 and modified as described in Section 3 above. Care was taken to ensure that the region was searched on a grid finer than the Nyquist frequencies to ensure complete sampling of the χ^2 plane. In the case of the *ROSAT* data, we have included the 1993, 1994 and 1996 data, with a total timespan of 3 years, similar to that for the *XMM-Newton* data, while the two *Chandra* observations span ~ 20 months. This resulted in MLPs with dimensions of 2000×2000 , with datasets of 1.4×10^6 , 8×10^4

and 2×10^4 events in the case of *XMM-Newton*, *Chandra* and *ROSAT* respectively.

The results are shown in Figure 4. The outer contours are the 99% confidence intervals for two parameters of interest, except for the *XMM-Newton* MLP where contours to include 99.9% significance are shown for illustration. The *Chandra* MLP shows diagonal alias patterns resulting from the availability of data at only two epochs. The *ROSAT* MLP consists of two main diagonals, broken into regions of better and less good fit, together with a lower likelihood contour parallel to these at shorter periods. In the case of the *XMM-Newton* MLP there are five regions, although at the 99% confidence level, only the central upper left region is significant.

Overlaying these MLPs, it is clear that there is no single location at which all three datasets intersect. The consequence is that there is an inconsistency between the three determinations. In particular, the $[P_0, \dot{P}]$ contours from the *XMM-Newton* MLP do not intersect with those of either the *ROSAT* or *Chandra* MLPs. This has persisted, despite an exhaustive reassessment of the analysis.

5.2 Simulated data

In order to investigate the viability of the coherent analysis (K02 questioned the applicability of approach in the study by Z02) and to verify more stringently the analysis process, we have generated simulated data with the same mean levels, noise characteristics and observation durations as the real data in Table 1. For those observations which were broken into several shorter sections (such as the *Chandra* and the *ROSAT* data), the simulated data were generated similarly. An intensity variation of linearly increasing period, with P_0 and \dot{P} similar to that deduced from the incoherent analysis was introduced into the data. The simulated dataset therefore closely matched the real dataset, with the difference that the P_0 and \dot{P} were known, and the time reference for all the data was known with certainty to be common. These data were phase folded using equation (4) and the known P_0, \dot{P} , and it was checked that all data co-phased correctly.

We proceeded with the analysis as follows. The $[P_0, \dot{P}]$ plane bounded by $[8.391050 - 8.391120, 0 - 2 \times 10^{-13}]$ was searched using the MLP, first coherently within the Ch00 and X00a,b datasets, then in the Ch01 and X02a,b datasets and finally in the R96 datasets. Each search resulted in a diagonal set of contours in $\Delta\chi^2$, corresponding to the alias patterns. We verified that the known $[P_0, \dot{P}]$ lay on one of the best-fit valleys. The orientation of the contours is increasingly angled with time, so that overlaying the three 2-dimensional MLPs identified a limited number of locations where the three datasets gave best fits. We confirmed this more quantitatively by a simple multiplication of the three MLPs. One of these loci (but not quite the minimum) was the input $[P_0, \dot{P}]$. We then carried out a coherent MLP analysis of all of the R96, Ch00, X00a,b, Ch01, and X02a,b datasets in the limited $[P_0, \dot{P}]$ spaces around these loci. This coherent analysis generated the $\Delta\chi^2$ values requiring mutual co-phasing of all of the datasets, and now the minimum in the plane was found indeed to coincide with the input $[P_0, \dot{P}]$.

This exercise verified both the MLP analysis routines

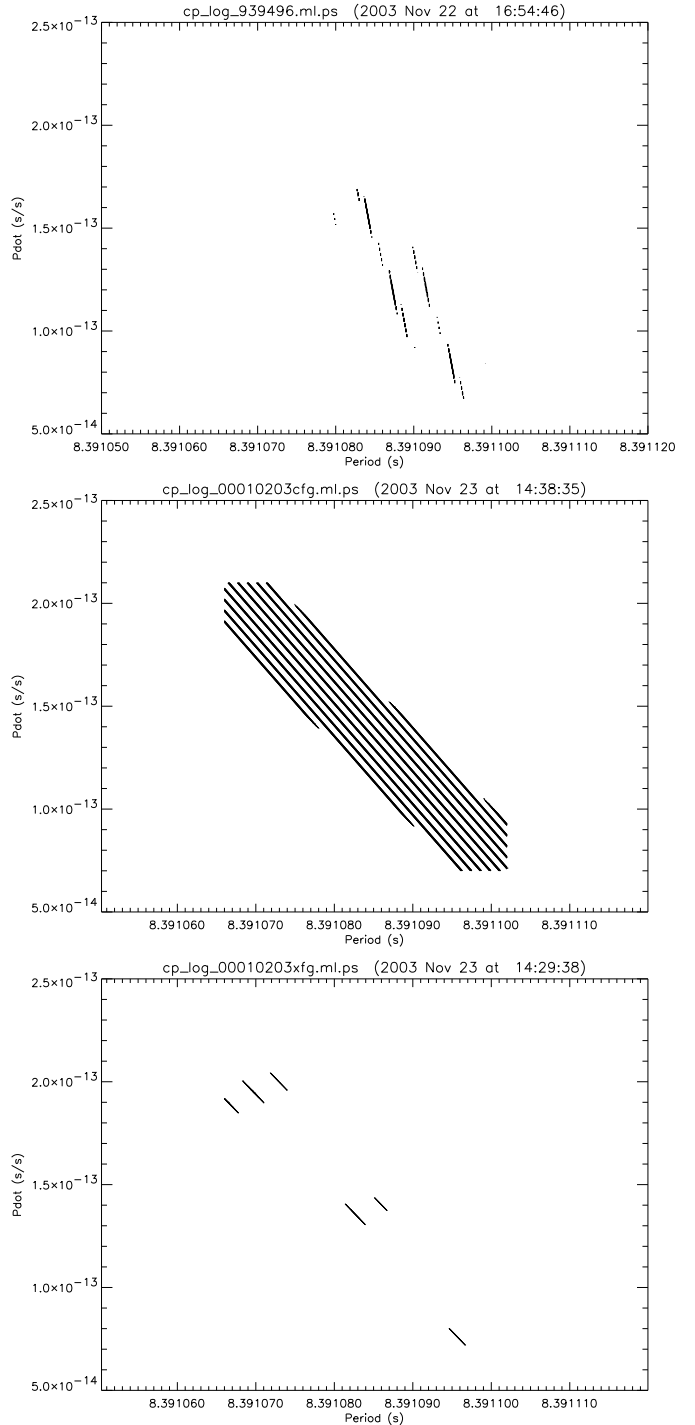


Figure 4. Contours of $\Delta\chi^2$ in the $[P_0, \dot{P}]$ plane for the R93, R94 and R96 dataset (top) for the Ch00 and Ch01 dataset (centre) and the X00, X02 and X03 dataset (bottom). In the *XMM-Newton* data, were the 99% confidence interval contours (rather than the 99.9% in this case) only to be shown, then only the central region at the top left is significant.

in as realistic fashion as possible, and the feasibility of identifying the correct period amongst the alias patterns, given the nature of the particular datasets at hand.

We repeated this order of analysis for the real datasets. Overlaying the MLPs identifies three loci where there is overlap in the patterns, around $[8.3910771, 1.796 \times 10^{-13}]$, $[8.3910954, 9.50 \times 10^{-14}]$ and $[8.3910865, 1.3825 \times 10^{-13}]$. A detailed search using the entire dataset identifies the region around the first solution as the only region where a coherent phase can be maintained over the entire dataset. The best fitting $[P_0, \dot{P}] = [8.39107712, 1.7956 \times 10^{-13}]$. However, when folded, this $[P_0, \dot{P}]$ pair is inconsistent with the X03 dataset.

5.3 Possible origins for the discrepancy

At this stage we are not able to arrive at a consistent coherent solution for a $[P_0, \dot{P}]$ pair from our extensive dataset. However: firstly, we have shown from the simulations above that the dataset *in principle* contains sufficient information to identify the correct solution, even if we do not include data from the X03 observations, or from S97, R93 or RASS datasets. Therefore, if a solution with \dot{P} constant does exist, the technique based on the coherent analysis allows us to identify it. Secondly, we have also verified that the software used to calculate the MLP returns the input parameters for the simulation correctly: we believe that any coding errors are therefore unlikely. Thirdly, in our analysis in Section 5.1 we have taken care not to mix the data from different satellites, so we have avoided any residual difficulties in relating the different time systems used for the different satellites.

Consequently we conclude that either the event timings used in our data are incorrectly assigned with respect to observations at other epochs with the *same* satellite, or that the model we have used for a constant period change [equation (5)] is inappropriate. We discuss these in turn.

We have cross-checked the event timings for our data where they overlap with K02. K02 have revised their table 1 post-publication, in the version held on the Astro-ph server which corrects the time system reference and other errors used to calculate their ToAs in their published version. We have carried out a detailed cross-check between the ToAs in their revised table and our datasets in Table 1. Our ToAs are given in Table 2. For those datasets in common (R93, R96d, S97, Ch00 and Ch01), the ToAs we calculate match those derived by K02 closely (to within 2% of the period), and we derive similar uncertainties. This indicates that these independently-derived datasets have been reduced consistently, and the likelihood of systematic errors remaining is now small. However, it is impossible to eliminate the possibility of error entirely since similar misconceptions could be resident in the software, or use of the software, for reducing the data – such as was the cause of the error in relating *ROSAT* and *Chandra* data in Z02 and K02.

In the case of the *XMM-Newton* timings, no such cross-check is currently possible. It is also of some concern that the best fit $[P_0, \dot{P}]$ pair from the *XMM-Newton* observations alone (top centre contours in Figure 4) are located outside of the 90% confidence intervals calculated from the incoherent analysis (Figure 3). We have therefore investigated the timing accuracy of *XMM-Newton* in further detail. After the *XMM-Newton* SAS *barycen* task was corrected for version

13.1, an absolute time shift in Crab pulsar data of ~ 1.2 msec remained with respect to the radio data. This resulted from an incorrect sign used to compensate for internal electronic delays. Becker (private communication) reports that there is still a time difference of between 600 and 300 μ sec in the Crab data (apparently decreasing with time) so minor timing discrepancies remain.

These discrepancies appear to be on such a scale that they would not affect our *XMM-Newton* analysis. However, there is some indication that there may be larger scale discrepancies inherent in some *XMM-Newton* datasets. These have arisen in some eclipsing binary data, for example OY Car (Wheatley & West 2003), and in EP Dra (Bridge 2004). In the former case, the eclipse occurs 55 sec early, while in the latter it occurs 69 sec late. These residuals are significantly larger than permitted by the uncertainties in the ephemerides for the two stars and would invalidate the coherent analysis for our *XMM-Newton* datasets of RX J0720.4–3125. Schwobe et al. (2004) also find some timing discrepancies for DP Leo, but report on the other hand that the eclipses in *XMM-Newton* observations of HU Aqr are consistent with the orbital ephemeris. The situation remains unclear.

Regarding the appropriateness of a constant \dot{P} model [equation (5)], we note three possibilities: glitching may have occurred, or there may be a deviation from a constant spin down, or a modulation in arrival times due to the star being in a binary system. Glitching behaviour has been observed in neutron stars with spin periods as long as that of RX J0720.4–3125, as for example in the anomalous X-ray pulsars (AXP) 1E2259.1+586 and 1RXS 1708–4009. Long term monitoring of several AXPs with the *Rossi X-ray Timing Explorer* (Kaspi et al. 2001, Gotthelf et al. 2002, Gavril & Kaspi 2002) revealed the diversity in the behavior of the single objects, ranging from high stability (in 1E2259.1+586 in quiescence, and 4U 0142+61 for which a linear fit with constant $\dot{\nu}$ phase-connects data collected over more than 4 years) to instabilities so severe that phase-coherent timing is not possible (as in 1E 1048.1–5937). In the case of AXPs, timing stability decreases with increasing $\dot{\nu}$ and the frequency derivative of RX J0720.4–3125 is one order of magnitude lower than that of the most stable AXPs. However, since the two sources belong to different classes of pulsars, it is not really obvious how much the extrapolation of this trend can be trusted.

So far, regrettably the sampling of the current dataset is not likely to be sufficient to distinguish whether either of these possibilities is the explanation for the inconsistencies we obtain in our MLPs.

5.4 Combined analysis

As discussed in § 5.1, we cannot find a consistent single $[P_0, \dot{P}]$ pair from the analysis of the datasets from different satellites. However, there is an overlap between the *ROSAT* and *Chandra* MLPs, therefore it is possible to compute a coherent MLP by restricting the analysis only to these data. The agreement in ToAs computed by K02 and ourselves here suggests that errors in the event timings are unlikely. Owing to the sparseness of the sampling, six aliases remain in the coherent analysis. These all have $1.1 \times 10^{-13} < \dot{P} < 1.65 \times 10^{-13}$ and are shown in Figure 5(a).

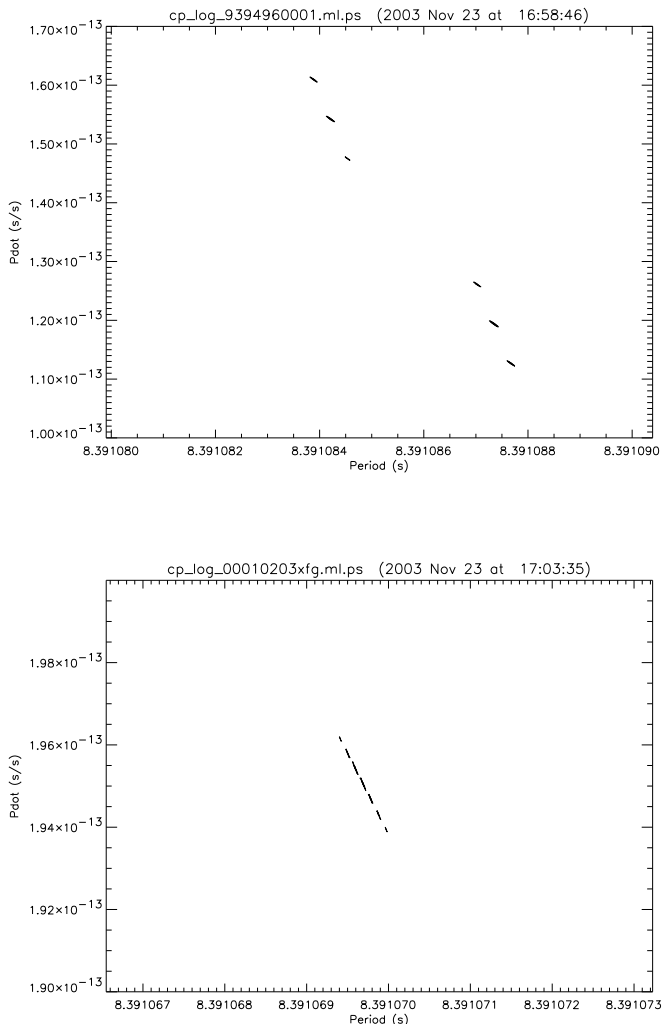


Figure 5. The final 99% confidence contours for the coherent analysis of the combined R93, R94, R96, Ch00 and Ch01 datasets (top) and those for the coherent analysis of the *XMM-Newton* datasets in more detail (bottom). In the bottom panel, the apparent aliases are the result of the contouring software.

The *XMM-Newton* dataset is the largest and provides highest S/N ratio MLPs. If we take it at face value, a region with $\dot{P} \sim 1.95 \times 10^{-13}$ is identified in the MLP. This is shown in Figure 5(b).

5.5 The incoherent analysis revisited

In the light of the above uncertainties, it is necessary to examine whether the incoherent analysis presented in Section 4 has been compromised. We consider this unlikely, because the precision derived from a coherent analysis of the time spanned by our data is nearly two orders of magnitude greater than that which can be derived from the incoherent analysis. The incoherent analysis is therefore unlikely to be affected by the uncertainties at the accuracy required for it. The incoherent analysis is also immune from many sources of error which might come to light only when data from different epochs are combined, such as might arise for light

travel time corrections, or the transformation between time systems.

6 DISCUSSION

6.1 Interpretation of the spin down rate

We have presented a revision of the measure of the RX J0720.4–3125 spin down rate published last year by Z02. By using additional *Chandra* and *XMM-Newton* datasets, we have been able to determine a *positive* spin down rate of $\dot{P} = (1.4 \pm 0.6) \times 10^{-13}$ s/s at 99% confidence level, as derived from the incoherent analysis. More refined values have been derived from a coherent analysis, separating *ROSAT* and *Chandra* datasets from the *XMM-Newton* ones. However, a self-consistent phase-coherent solution based on the entire set of data from the three different satellites cannot be found. Due to these unresolved issues, in order to discuss the physical implications of our measure we concentrate on the result obtained from the incoherent analysis. Because of the larger numbers of datasets available since Z02 and K02, this measure of the spin-down rate is now sufficiently constraining for our needs.

Despite the fact that the value of \dot{P} reported here is higher than in Z02, the two solutions are sufficiently similar that most of the scientific conclusions published by Z02 remain unchanged.

First of all, our measure rules out the possibility that the source is accreting from the interstellar medium, since this requires $\dot{P} < 10^{-15}$ s/s (see Z02, K02).

Furthermore, makes it unlikely that RX J0720.4–3125 is spinning down under propeller torques exerted by the interstellar medium. In Z02 our argument against this was based on the combination of two constraints between magnetic field, density of the medium and star velocity. The first was obtained from the expression of the propeller spin down, and the second by imposing that the star has entered the propeller phase. The latter gives $B_{12} < 25\sqrt{n}v_{10}^{-3/2}$, where n is the external density in cm^{-3} , $B_{12} = B/(10^{12} \text{ G})$ and v_{10} is the star’s velocity normalized to 10 km/s. For the former condition we used a propeller model as in Colpi et al. (1998)

$$\dot{P}_{prop} \approx 10^{-8} n^{9/13} v_{10}^{-27/13} B_{12}^{8/13} P^{21/13} \frac{\text{s}}{\text{yr}}, \quad (7)$$

that, for $\dot{P} = (1.4 \pm 0.6) \times 10^{-13}$ s/s, gives $B_{12} \approx (36 - 139)n^{-9/8} v_{10}^{27/8}$. Therefore, the two conditions taken together limit the star’s velocity to $v_{10} \lesssim n^{1/3}$ ($n \sim 1$ for the interstellar medium). This modest velocity was regarded as unlikely at the time of the Z02 paper, and it is now ruled out by the recent measure of a proper motion of 97 ± 12 mas per year (Motch, Zavlin & Haberl, 2003), which corresponds to a transverse velocity $V_T \sim 50 \times (D/100pc)$ km/s. Since v_{10} is likely to be greater than unity, the propeller mechanism dominates only if the star is presently going through a high density medium, with $n > 100$. The possibility that RX J0720.4–3125 is passing through one of these high density clouds (which are suggested to be present on small scales ranging from 10 to 10^6 AU, see Lauroesch & Meyer 2000) has been considered by Motch et al. (2003). However, their conclusion is that this scenario is problematic since it may imply changes in the X-ray flux and blackbody tempera-

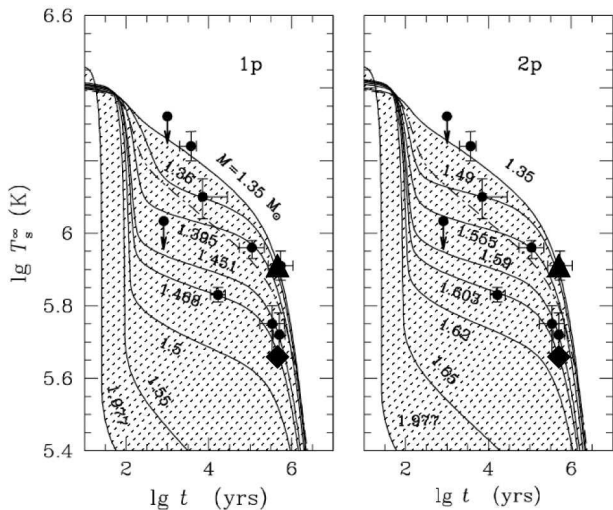


Figure 6. The location of 9 isolated neutron stars in the temperature/age diagram for two different models of proton superfluidity (1p and 2p) and different masses (figure adapted from Yakovlev et al. 2003). In both panels, the diamond and the triangle mark the position of RX J0720.4–3125 as obtained assuming $T^\infty = 0.4 \times 10^6$ K and $T^\infty \sim 0.9 \times 10^6$ K, respectively (see text for details)

ture (not observed so far) and it cannot account for a large $\dot{P} > 10^{-14}$ s/s.

We are then left with two possible explanations for the cause of the observed spin down rate: propeller torque exerted by a fossil disk or spin down due to emission of magnetic dipole radiation. Although the first cannot be completely ruled out by our measure, and may better explain a high level of timing noise which is typical of accretors (Kaspi et al. 2001), we regard it as extremely unlikely. In fact, it requires two separate mechanisms to explain the observed X-ray luminosity and spin down rate (see Z02). Also, as discussed by Perna et al. (2000) (see also Kaplan et al. 2003), disk models fail in modeling the spectrum of the optical counterpart.

By interpreting the spin down rate in terms of magnetic radiation losses and assuming a dipolar field we can constrain the spin down age, $t_{sd} = \dot{P}/(2P) \sim (0.6 - 1.5) \times 10^6$ yr, and the present value of the magnetic field, $B = (2.8 - 4.2) \times 10^{13}$ G.² The spin down age is consistent with the flight time of 10^6 yrs from the two birth places proposed by Motch et al. (2003), the Sco OB2 complex and the Vela OB2 + Trumpler 10 association.

6.2 Location in the temperature/age diagram and estimate of the mass

The age derived from our timing analysis can be then compared with the star’s age as inferred by the cooling curves,

² As in Z02, we reiterate that this must be regarded as an upper limit. A twisted magnetosphere may lead to a reduction up to an order of magnitude in the inferred polar value of the magnetic field. The estimate of the spin down age is unaffected (Thompson, Lyutikov & Kulkarni, 2001).

which is based on the spectral measure of the surface temperature.

Different theoretical cooling models have been presented in the literature. Roughly speaking, they predict a two-fold behavior of the cooling curves: slow cooling for low-mass neutron stars and fast cooling for stars with higher masses. The transition between the two regimes can be more or less sharp, depending on the assumed superfluid properties of the neutron star interior. It has been realized (see Yakovlev et al., 2003 for a recent discussion) that simple models which do not account for proton and neutron superfluidity fail in explaining the surface temperatures observed in many sources, unless there is a fine tuning in the masses of objects such as Vela, Geminga and RX J1856–3754, and all of them have nearly the critical mass that bounds the (in this case, sharp) transition between slow and fast cooling regimes. Models with proton superfluidity included do not require this unlikely assumption and predict the existence of a region, intermediate between the two regimes and relatively large in the parameter space, which is populated by medium mass neutron stars (roughly between 1.4 and 1.65 M_\odot). Although the full picture only holds if, at the same time, neutron superfluidity is rather weak, so far the latter models provide a better comparison with observations. It is interesting that many neutron stars (as 1E 1207–52, Vela, RX J1856–3754, PSR 0656+14) have a surface temperature which falls in such a transition region (see Figure 6, re-adapted from Yakovlev et al., 2003).

If the origin of the X-ray flux from RX J0720.4–3125 is the thermal emission from the cooling neutron star, in first approximation the surface temperature can be taken equal to the temperature of the blackbody fit, i.e. $T^\infty \sim 0.9 \times 10^6$ K (Haberl et al., 1997; Paerels et al., 2001; Haberl et al., 2004). This is likely to be an upper limit, since most detailed atmospheric models or fits which account for a broad-band deviation from a blackbody tend to give a smaller temperature (see e.g. Pavlov et al., 2002; Burwitz et al., 2003). As we can see from Figure 6, this gives a maximum cooling age of $\sim 0.3 \times 10^6$ yr (for $M \sim 1.35 M_\odot$) which, given the numerous uncertainties, may be considered as marginally compatible with the spin-down age. Alternatively, Kaplan et al. (2003) propose a multicomponent fit to optical/X-ray data of RX J0720.4–3125 concluding that the X-ray emission at $\sim 0.9 \times 10^6$ K originates from hot polar caps, while the whole surface is cooler with a blackbody temperature of $T^\infty \sim 0.4 \times 10^6$ K. If this is the case, the spin down age is compatible with RX J0720.4–3125 being a medium mass neutron star with $M \sim 1.5 - 1.6 M_\odot$, depending on the kind of proton superfluidity assumed in the model (1p and 2p respectively).

It is worth noting that given the significant spread in the cooling curves in Figure 6 resulting from a strong mass dependence, an age as low as 10^4 yr (which may be possible if the magnetic field decays rapidly) is also consistent with the observed surface temperature. We discuss these issues in the next section.

6.3 Implications for the past history of RX J0720.4–3125

The considerations presented so far are based on the spin down age t_{sd} , which is representative of the true age of the

source only in the case in which the magnetic field has remained almost constant during the star evolution. The same condition applies for the validity of the cooling curves mentioned above, which do not include the extra input of energy released in the neutron star in case of field decay. Taken face value, the timing parameters of RX J0720.4–3125 are compatible either with those of a radio-quiet cooling pulsar with high (but not extreme) magnetic field or an old magnetar, born with $B > 10^{14}$ G and still kept warm by the decay of its superstrong field. As in Z02, in order to discriminate between these possibilities, we studied the evolutionary tracks on the B, \dot{P} diagram. Three different mechanisms are typically proposed for inducing field-decay: ambipolar diffusion in the solenoidal or irrotational mode and Hall cascade (Goldreich & Reisenegger 1992, Heyl & Kulkarni 1998, Colpi, Geppert & Page 2000). In reality all the three processes co-exist with different time scales, and each of them may dominate the evolution depending on the instantaneous values of B, L . In absence of more detailed computations, Heyl & Kulkarni (1998) and Colpi, Geppert & Page (2000) tentatively isolated the three processes and proposed some simple, phenomenological rules to mimic the evolution in the three regimes. As in Z02, we used as first approximations these decay rules and re-computed the source age, τ_d , and the value of the magnetic field at the birth of the neutron star, B_0 corresponding to our revised measure of \dot{P} . By measuring B_0 in 10^{13} G, P in seconds, \dot{P} in s/yr and the age in 10^6 yr, the resulting expressions are

$$B_0 = (P\dot{P})^{1/2} \left[b^{\frac{\alpha-2}{2}} - \frac{\alpha-2}{2} \frac{a}{b} (P\dot{P})^{\frac{\alpha-2}{2}} (P^2 - P_o^2) \right]^{\frac{1}{2-\alpha}} \quad (8)$$

$$\tau_d = (a\alpha B_0^\alpha)^{-1} \left\{ \left[1 - \frac{2-\alpha}{2} \frac{a}{bB_0^{2-\alpha}} (P^2 - P_o^2) \right]^{\frac{\alpha}{\alpha-2}} - 1 \right\}, \quad (9)$$

where $b \approx 3$, P_0 is the period at the star birth, and the parameters a, α discriminate between the three decay laws (Colpi, Geppert & Page, 2000). The results are shown in Table 3. In all cases the star is assumed to be born with a period of 1 ms: results are not strongly dependent on this exact value, provided it is less than the present period³.

As we can see, the only scenario compatible with a superstrong field at the star’s birth ($B_0 \sim 10^{15}$ G) is that one involving a very fast decay, i.e. the Hall cascade. In this case the predicted star’s age is $\sim 4 \times 10^4$ yr. Although such a young age is only marginally compatible with the absence of a remnant, it is not incompatible with that inferred from the cooling curves (see Figure 6) provided the mass is slightly larger. A slightly larger mass still is required if we allow for the extra-heating due to B -decay from Hall cascade (Geppert & Colpi, private communication).

On the other hand, both mechanisms involving ambipolar diffusion predict a magnetic field which is relatively constant over the source lifetime and close to the present value. The corresponding star’s age is between $\approx 0.4 \times 10^6$ yr and $\approx 1.4 \times 10^6$ yr, and is close to τ_{sd} .

Solution	B-Decay Mechanism	B_0 10^{13} G	age (years)
1	Hall Cascade	120.2	3.5×10^4
1	Amb. diff., irrotational mode	3.0	1.4×10^6
1	Amb. diff., solenoidal mode	5.3	0.8×10^6
2	Hall Cascade	121.6	2.3×10^4
2	Amb. diff., irrotational mode	4.4	0.6×10^6
2	Amb. diff., solenoidal mode	7.0	0.4×10^6

Table 3. Predicted source age and primordial field for three different mechanisms of decay, simulated as in Colpi et al. (2000). Here $P = 8.391$ s, and we used different values of \dot{P} : $\dot{P} = 0.8 \times 10^{-14}$ s/s (solution ‘1’) and $\dot{P} = 2 \times 10^{-13}$ s/s (solution ‘2’). These correspond to the boundaries of the 99% confidence range derived from our coherent analysis. In all cases, the source is assumed to be born with $P = 1$ ms.

7 CONCLUSIONS

We have eliminated the discrepancies between the calculated ToAs in the K02 paper and those derived from the same data analysed by Z02. This invalidated our derived $[P_0, \dot{P}]$ solutions in Z02 (K02 have also updated their ToAs). In order to correct these solutions, we have reanalysed the datasets and taken the opportunity to incorporate significant new datasets from both *Chandra* and *XMM-Newton*. At the same time, we have revised the model used by Z02 to be fitted to the data to retain the correct phase reference.

Taken individually, the combination of old and new datasets allow a significantly more accurate $[P_0, \dot{P}]$ solution to be derived than that in K02 or Z02. This *establishes that RX J0720.4–3125 is spinning down*.

We have also attempted a phase-coherent analysis of the combined datasets, as in Z02. However, we have been unable to find a consistent solution, even when we analyse the data from different satellites separately. In this case the *XMM-Newton* data are not consistent with the other data. We have explored the possible reasons for this: they may be intrinsic to RX J0720.4–3125 (in which case the constant \dot{P} model is not appropriate), or they may result from continuing timing errors in the data we have not succeeded in identifying. We present the solutions from the combined *ROSAT* and *Chandra* data and the *XMM-Newton* data separately.

The individual (incoherent) $[P_0, \dot{P}]$ solution is sufficiently accurate to allow us to place strong constraints on the mechanism causing the spin-down. The large $\dot{P} \sim 10^{-13}$ s/s rules out accretion and propeller origins and points toward an interpretation in terms of magneto-dipolar braking. This in turn constrains the age of RX J0720.4–3125 and its magnetic field strength.

For a magnetic field as strong as $B = (2.8–4.2) \times 10^{13}$ G, the electron cyclotron line is inaccessible (it falls at about 350 keV). However, a relatively broad proton cyclotron absorption feature is predicted at $\approx 0.2–0.3$ keV (Zane et al., 2001). The presence of a cyclotron absorption line at the low energy of the sensitive energy band of the *XMM-Newton* EPIC instruments has been indeed recently reported (see Haberl et al., 2003a, 2004). The feature may explain the observed deviations from a Planckian shape at these energies, and possibly also the anticorrelation of the modulation of

³ K02 discuss the possibility that RX J0720.4–3125 is an example of the ‘injection’ hypothesis (Vivekanand & Narayan, 1981) and is born with a long period, $P_0 \sim 8.3$ s. In this case, all three decay laws predict an age of order 10^4 yr.

hardness ratio and total X-ray intensity detected by *XMM-Newton* (Cropper et al., 2001).

Our study allows a possible evolutionary link between dim INS and AXPs (which relies on the interpretation of the former as warm-out magnetars) but only if the INS have an age of $\sim 10^4$ yr. A more conservative interpretation is that RX J0720.4–3125 was born with a strong, but not super-strong, field [$B = (2.8 - 4.2) \times 10^{13}$ G] which is compatible with those of the canonical radio-pulsars. Similar conclusions have been argued also by K02, however their measure of \dot{P} has a large error and does not permit the discrimination between this and the separate possibilities that RX J0720.4–3125 has a more conventional field ($B \sim 10^{12}$ G) and lower spin-down rate ($\dot{P} \sim 10^{-15}$ s/s) or is even spinning-up. Comparing with the radio-active pulsar population, objects with $B > 10^{13}$ G are rare, but their evidence is rapidly growing (Camilo et al., 2000). The parameters of RX J0720.4–3125 we have derived are not too dissimilar from those of PSR J1814–1744, which has $P \sim 4$ s and $\dot{P} \sim 7.4 \times 10^{-13}$ s/s.

One of the most striking mysteries about *ROSAT* isolated neutron stars, AXPs, soft- γ repeaters and objects like Geminga is why they do not exhibit radio emission. As suggested by Motch et al. (2003), who derived very similar conclusions basing on the proper motion measurement, it could thus be that RX J0720.4–3125 and several others apparently radio-quiet neutron stars are just radio pulsars with off-axis beam that does not cross the Earth. The radio beam narrows with increasing periods (Briggs 1990), making this explanation even more plausible. On the other hand, evidence for a population of genuinely radio-silent young neutron stars arises from population synthesis (Neuhäuser & Trümper, 1999; Gotthelf & Vasisht, 2000; Popov et al., 2000a,b and references therein). The group of *ROSAT* INSs is very homogeneous and they are all relatively close-by (within 300-400 pc), making unplausible that all their beams are misaligned. At present, these two possibilities cannot be distinguished. Detailed timing analysis of other *ROSAT* INSs is crucial to reach a more comprehensive understanding of the entire population.

8 ACKNOWLEDGMENTS

We are grateful to Uwe Lammers for his reprocessing of the *XMM-Newton* ODFs. We thank David Kaplan for several discussions regarding the ToAs and for pointing out the difference between the event timings in his and our BeppoSAX data. We thank Marco Feroci for processing the BeppoSAX data, and Tim Oosterbroek and GianLuca Israel for providing information on the intricacies of the time correction in the SAX DAS. We also thank Werner Becker for his insights into the possible sources of error in the *XMM-Newton* timing.

REFERENCES

- Bridge, C.M., 2004, *Ph.D. Thesis*, University of London
- Briggs, J.D., 1990, *MNRAS*, 245, 514
- Burwitz, V., Haberl, F., Neuhäuser, R., et al., 2003, *A&A*, 399, 1109
- Camilo, F., Kaspi, V.M., Lyne, A.G., et al., 2000, *ApJ*, 541, 367
- Colpi, M., Turolla, R., Zane, S., et al., 1998, *ApJ*, 501, 252
- Colpi, M., Geppert, U., & Page, P., 2002, *ApJ*, 529, L29
- Cropper, M., Zane, S., Ramsay, G., Haberl, F. & Motch, C., 2001, *A&A*, 365, L302
- Gavriil, F.P., & Kaspi, V.M., 2002, *ApJ*, 567, 1067
- Goldreich, P. & Reisenegger, A., 1992, *ApJ*, 395, 250
- Gotthelf, E.V., & Vasisht, G., 2000, *Pulsar Astronomy and Beyond*, ASP Conference Series, vol. 3×10^8 , M.Kramer, N.Wex, and R. Wielebinski eds, astro-ph/9911344
- Gotthelf, E.V., Gavriil, F.P., Kaspi, V.M., et al., 2002, *ApJ*, 564, L31
- Haberl, F., Motch, C., Buckley, D. A. H., Zickgraf, F.-J., Pietsch, W., 1997, *A&A*, 326, 662
- Haberl, F., Schwöpe, A. D., Hambaryan, V., Hasinger, G., & Motch, C., 2003a, *A&A*, 403, L19
- Haberl, F., Zavlin, V. E., Trümper, J., & Burwitz, V. 2004, *A&A*, submitted, astro-ph/0312413
- Heyl, J.S. & Kulkarni, S.R., 1998, *ApJ*, 506, L61
- Kaplan, D. L., Kulkarni, S. R., van Kerkwijk, M. H., et al., 2002, *ApJ*, 570, L79. Also astro-ph/0205029 (revised version)
- Kaplan, D. L., van Kerkwijk, M. H., Marshall, H. L., et al., 2003, *ApJ*, 590, 1008
- Kaspi, V.M., Gavriil, F.P., Chakrabarty, D., et al., 2001, *ApJ*, 558, 253
- D. L., van Kerkwijk, M. H., Marshall, H. L., et al., 2003, *ApJ*, 590, 1008
- Kuster, M., 2001, reported at “New Visions of the X-ray Universe in the *XMM-Newton* and *Chandra* Era”
- Lauroesch, T.J., & Meyer, D.M., 2000, *ApJ*, 543, L43
- Motch, C., Zavlin, V.E., & Haberl, F., 2003, *A&A*, 408, 323
- Neuhäuser, R., & Trümper, J. E., 1999, *A&A*, 343, 151
- Perna, R., Hernquist, L., & Narayan, R., 2000, *ApJ*, 541, 350
- Paerels, F., Mori, K., Motch, C., Haberl, F., Zavlin, V.E., Zane, S., Ramsay, G., Cropper, M., 2001, *A&A*, 365, 302
- Pavlov, G.G., Zavlin, V.E., & Sanwal, D., 2002, *Proceedings of the 270. WE-Heraeus Seminar on: “Neutron Stars, Pulsars and Supernova Remnants”*, Physikzentrum Bad Honnef, Germany, eds. W.Becker, H.Lesh, & J. Trümper, MPE Report 278, pp. 273-286
- Popov, S. B., Colpi, M., Treves, A., et al., 2000a, *ApJ*, 530, 896
- Popov, S. B., Colpi, M., Prokhorov, M. E., et al., 2000b, *ApJ*, 544, L53
- Schwöpe, A., Hambarayan, V., Staude, A., et al., 2004, *ASP Conference Series*, IAU Coll. 190, eds Vriellmann, S., Cropper, M., In press
- Thompson, C., Lyutikov, M. & Kulkarni, S.R., 2001, *ApJ* submitted (astro-ph/0110677)
- Vivekanand M. & Narayan, N., 1981, *Journal of Astrophysics and Astronomy*, 2, 315
- Wheatley, P., West, R. G., 2003, *MNRAS*, 345, 1009
- Yakovlev, D.G., Gnedin, O.Y., Kaminker, A.D., et al., 2003, *Proceedings of the 34th COSPAR Scientific Assembly (Adv. Sp. Res., accepted)*, astro-ph/0306143
- Zane, S., Turolla, R., Stella, L., & Treves, A., 2001, *ApJ*, 560, 384
- Zane, S., Haberl, F., Cropper, M., et al., 2002, *MNRAS*, 334, 345

Zavlin, V. E., Pavlov, G. G., Sanwal, D., Trümper, J., 2000,
ApJ, 540, L25